iScience

CellPress
OPEN ACCESS

Article

Ketamine induced gut microbiota dysbiosis and barrier and hippocampal dysfunction in rats

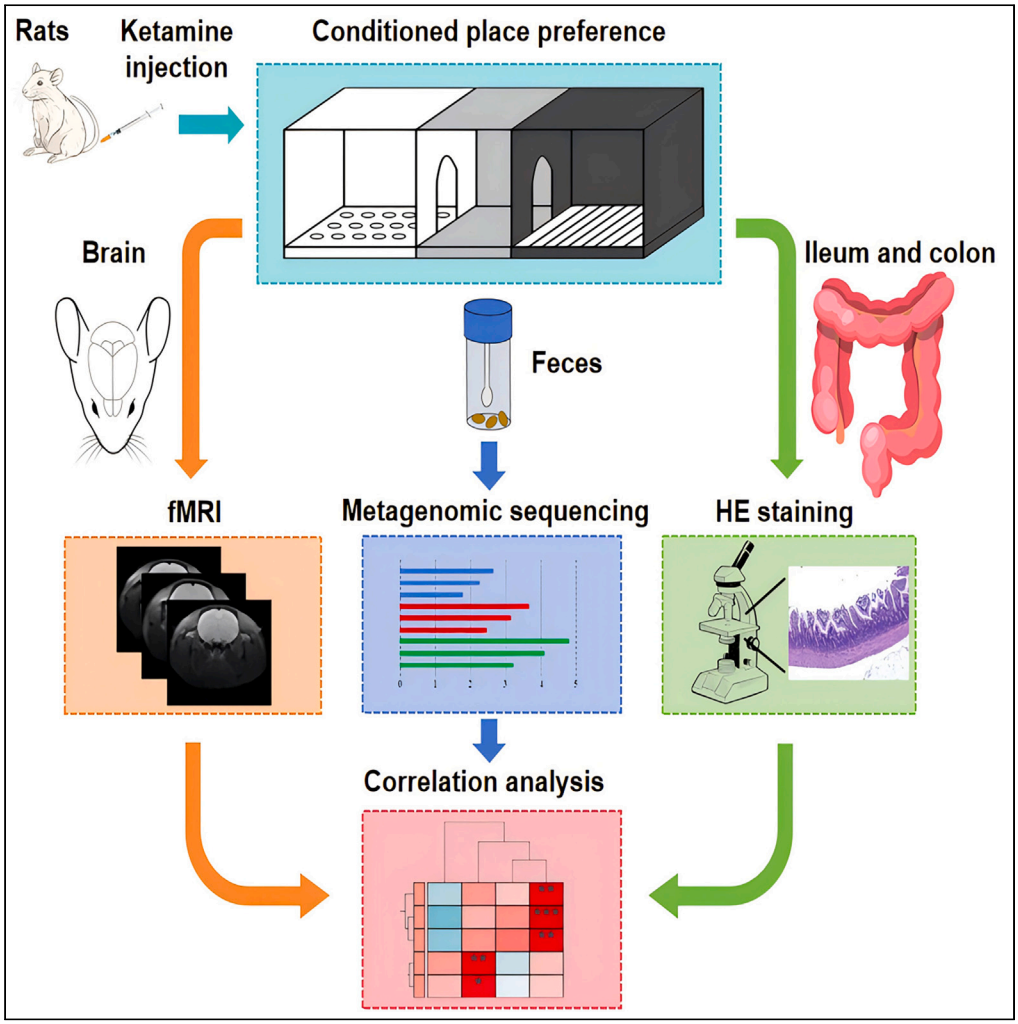

Lei Xie, Zelin Zhuang, Baowen Guo, ..., Yanmin Zheng, Renhua Wu, Shuhua Ma

rhwu@stu.edu.cn (R.W.)
shma@stu.edu.cn (S.M.)

Highlights

Ketamine induces alterations in gut microbiota, intestinal barrier, and brain function in rats

Hippocampal dysfunction correlates with gut microbiota and barrier of ketamine-CPP-addicted rats

Our findings provide insights into the role of microbiota-gut-brain axis in ketamine addiction

Xie et al., iScience *27*, 111089
November 15, 2024
https://doi.org/10.1016/j.isci.2024.111089

iScience

CellPress
OPEN ACCESS

Article

Ketamine induced gut microbiota dysbiosis and barrier and hippocampal dysfunction in rats

Lei Xie,[1,2,4] Zelin Zhuang,[1,2,4] Baowen Guo,[1,2,4] Yuehua Huang,[1,2] Xiaoyan Shi,[1] Zikai Huang,[1,2] Ziquan Xu,[1,2] Yanbin Chen,[1,2] Yuyin Cao,[1,2] Yanmin Zheng,[1,2] Renhua Wu,[3,*] and Shuhua Ma[1,2,5,*]

SUMMARY

The microbiota-gut-brain axis (MGBA) plays a pivotal role in drug addiction. However, the pathophysiological mechanism of MGBA in ketamine addiction remains elusive. The present study investigated the ketamine-induced gut microbiota disorders, intestinal barrier dysfunction, and the alterations in brain function, using a conditioned place preference (CPP) model of ketamine addiction in rats. Compared with the control group, ketamine induced decreased amplitude of low-frequency fluctuation (ALFF) values in the hippocampus, and pyknotic nuclei and concentrated cytoplasm in hippocampal neurons, as well as alterations in gut microbiota composition, shortened ileum villi, and thinner colonic mucosa. We also found that the abundance of gut microbiota exhibited correlations with CPP score, hippocampal ALFF value, length of ileum villi, and thickness of colonic mucosa. Our findings provide evidence for abnormal alterations in the MGBA of ketamine-addicted rats, which improves our understating of the mechanism of ketamine addiction and the potential for developing new therapeutic strategies.

INTRODUCTION

Ketamine is extensively employed as an anesthetic and analgesic agent in both clinical and research domains, which was initially synthesized in 1962 by Calvin Stevens of Parke-Davis Pharmaceuticals.[1] Due to its reinforcing and dissociative properties, ketamine induces severe drug dependence and intense craving, thereby promoting its abuse. The non-medical use of ketamine has shown a steady global increase over the past few decades,[2,3] and drug abuse presents a significant public health crisis, imposing substantial personal, economic, and social burdens.[4] Consequently, additional investigation into the underlying pathogenesis and exploration of effective interventions is imperative.

Magnetic resonance imaging (MRI) is essential for evaluating the structural, functional, and metabolic changes in brain tissue. Blood-oxygen-level-dependent functional magnetic resonance imaging (BOLD-fMRI), developed by Ogawa in 1990,[5] has been widely used in research on drug addiction. In the field of substance addiction, research utilizing fMRI has shown that rats exhibit increased signaling in regions such as the hippocampus, prefrontal cortex, nucleus accumbens, and thalamus following acute injection of varying doses of cocaine. Conversely, upon repeated exposure to cocaine, a decrease in signaling in brain regions, including the prefrontal cortex, nucleus accumbens, and dorsal thalamus, has been observed. This reduction was found to be unrelated to cerebrovascular activity, suggesting a decrease in functional nerve cell activity.[6]

The bidirectional signal transduction of the microbiota-gut-brain axis (MGBA) is implicated in the pathogenesis of drug addiction. Gut microbiota and its metabolites can modulate the central nervous system and modify brain function through metabolic, endocrine, immune, and neural pathways, thereby impacting cognitive function, emotion, and behavior.[7] Numerous studies have demonstrated significant alterations in the gut microbiota associated with drug addiction. Additionally, animal models suggest that the gut microbiota may play a role in influencing the response to drug addiction.[8–10]

While the significance of MGBA in the pathology of drug addiction is well established, the pathophysiological mechanisms underlying the interaction between gut microbiota and central nervous system (CNS) changes in ketamine addiction remain unclear. This study primarily employs the amplitude of low-frequency fluctuation (ALFF) analysis of MRI and metagenomic sequencing technology, supplemented by hematoxylin and eosin (H&E) staining, to investigate alterations in brain functional activity, intestinal microorganisms, and intestinal morphology in ketamine-addicted rats. The aim is to elucidate their correlations and provide a perspective and foundation for further research on ketamine addiction.

[1]Department of Radiology, The First Affiliated Hospital of Shantou University Medical College, Shantou 515041, China
[2]Laboratory of Molecular Imaging & Laboratory of Molecular Cardiology, The First Affiliated Hospital of Shantou University Medical College, Shantou 515041, China
[3]Department of Radiology, The Second Affiliated Hospital, Medical College of Shantou University, Shantou, China
[4]These authors contributed equally
[5]Lead contact
*Correspondence: rhwu@stu.edu.cn (R.W.), shma@stu.edu.cn (S.M.)
https://doi.org/10.1016/j.isci.2024.111089

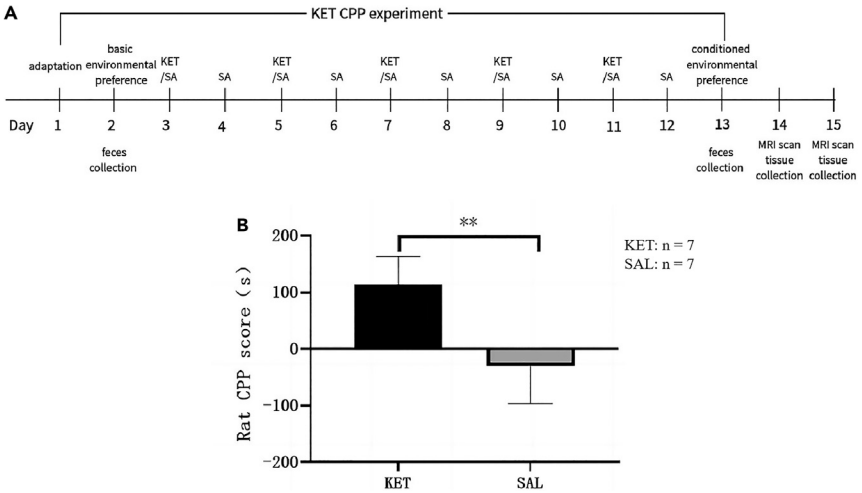

Figure 1. The CPP model experimental procedure and the results of CPP scores between the two group after modeling in rats (n = 7/7)

(A) The CPP model experimental procedure.

(B) The CPP score of rats in the KET group was higher than that of the SAL group. The data were analyzed with the Mann-Whitney U test and shown as the mean ± SD, **$p < 0.01$. CPP, conditioned place preference; KET, ketamine; SAL, saline.

RESULTS

Establishment of conditioned place preference model of ketamine addiction in rats

The CPP experiment spanned 13 days, as illustrated in Figure 1A. The CPP score of rats in the KET group was higher than that of the SAL group. The Mann-Whitney (U) rank-sum test results indicated a statistically significant difference ($p = 0.002$), as depicted in Figure 1B, confirming the successful establishment of the ketamine addiction rat model.

Intergroup differences in ALFF values in brain regions of resting-state functional MRI in rats

The ketamine addiction rats in the KET group exhibited increased ALFF values in the prefrontal cortex, orbitofrontal cortex, frontal association cortex, and retrosplenial cortex and decreased ALFF values in the hippocampus, lateral thalamic nuclei, and dentate gyrus (Table 1; Figure 2, $p < 0.005$, cluster level >20).

Detection by metagenomics of gut microbiota in rat feces

In this study, principal coordinate analysis (PCoA) was employed to analyze the microbial composition of the KET group and SAL group before and after CPP modeling. The results demonstrated a statistically significant difference in the overall comparison of microbial community composition among the two groups before and after CPP modeling ($p < 0.01$, Figure 3A). Furthermore, after CPP modeling, the community composition in the KET group showed significant alterations compared to the SAL group ($p < 0.05$, Figure 3B).

To identify characteristic microbes at the genus level in each group, linear discriminant analysis effect size (LEfSe) was utilized to test the significance of genus-level differences in the composition of gut microbiota among the four groups. Compared with other groups, the main bacterial flora in the KET group, after CPP modeling, included Akkermansia, Romboutsia, Avibacterium, Corynebacterium, Jeotgalibaca, Catenibacterium, Auritidibacter, Lysinibacillus, Enterococcus, Micromonospora, Intestinimonas, Mammaliicoccus, Trueperella, Oscillibacter, Desulfovibrio, Roseburia, Butyrivibrio, Jeotgalicoccus, Rodentibacter, Oligella, Salinicoccus, Dehalococcoides, Aerococcus, and Brevibacterium ($p < 0.05$, Figure 3C).

Morphological changes of hippocampal neurons, ileal villi, and colonic mucosa in rats

Under a 20× light microscope, H&E-stained sections of rat brains revealed that the hippocampal tissue structure in the SAL group was predominantly intact, with centrally located and clear neuron nuclei and rich, lightly stained cytoplasm. In contrast, hippocampal tissue from the KET group displayed a similar clear structure, but with some neurons exhibiting irregular morphology, condensed cytoplasm, and pyknosis, suggestive of apoptotic changes (Figures 4A and 4B). Under a 10× light microscope, H&E staining of the ileum and colon revealed that, compared to the control group, rats in the ketamine group exhibited a statistically significant decrease in the length of ileal villi and a thinner colon mucosa ($p < 0.01$, Figures 4C–4H; Table 2).

Correlation analysis between the abundance of gut microbiota and CPP score, hippocampal ALFF value, length of ileum villi, and thickness of colonic mucosa in ketamine-addicted rats

In the correlation analysis at the microbiota genus level, CPP scores exhibited primarily negative correlations with the abundance of Blastococcus and Alcaligenes and positive correlations with the abundance of Brachyspira, Filifactor, Fenollaria, Parolsenella, Parabacteroides,

Table 1. Differences in ALFF values between the ketamine addiction group and saline control group in rats

Condition	Brain region	L/R	Cluster size (voxels)	X	Y	Z	T value
ALFF (KET > SAL)	Frontal association cortex	L	12	0.5938	5.2658	−5.6379	3.5582
	Retrosplenial cortex	L	13	0.5938	5.1242	−5.6379	3.5735
	Prefrontal cortex	L	20	2.3543	6.6202	−6.5979	3.7222
ALFF (KET < SAL)	Hippocampus	R	3	4.3479	7.3944	−5.6379	−3.4131
	Lateral thalamic nucleus group	R	21	4.0777	7.7042	−6.1179	−4.0089
	Dentate gyrus	R	35	4.0777	8.0051	−6.1179	−4.2443

Two sample t tests; $p < 0.005$, cluster level>20; L, left; R, right; KET, ketamine; SAL, saline.

Holdemania, Saccharomonospora, Prevotellamassilia, Desulfitobacterium, Phoenicibacter, and Parascardovia. ALFF values of the hippocampus were mainly positively correlated with the abundance of Frigoribacterium, Kocuria, Methylobacterium, Arabiibacter, Catenibacterium, Nosocomiicoccus, Leucobacter, Eggerthella, and Syntrophobotulus. Conversely, the length of ileal villi primarily exhibited negative correlations with the abundance of Methylobacterium, Nosocomiicoccus, Leucobacter, Eggerthella, Ornithinimicrobium, Syntrophobotulus, and Enterorhabdus. The thickness of the colonic mucosa was mainly negatively correlated with the abundance of Bacillus, Nosocomiicoccus, Lacrimispora, and Mediterraneibacter, whereas it was positively correlated with the abundance of Sporosarcina, Clavibacter, and Paraclostridium ($p < 0.05$, Figure 5). Furthermore, Pearson correlation analysis revealed a negative correlation between ileal villus length and hippocampal ALFF value ($r = -0.96$, $p < 0.01$, Figure 6).

DISCUSSION

Due to its capacity for mental stimulation and rapid absorption, ketamine can induce central excitement and hallucinations. However, it also demonstrates significant potential for inducing mental dependence and abuse, thereby posing a substantial threat to public health, social stability, and the overall well-being of individuals.[11] The importance of understanding the bidirectional communication pathway of the MGBA is increasingly acknowledged. Accumulating evidence suggests that drug addiction can modulate the composition of gut microbiota, whereas gut microbiota may, in turn, influence susceptibility to drug addiction. In this study, we employed the ALFF analysis of resting-state functional MRI to examine the local brain functional activity changes, metagenomic sequencing technology was used to investigate alterations of the gut microbiota composition, and H&E staining was used to detect the brain and intestinal morphology in model rats. Our findings aim to establish a theoretical framework for comprehending their interrelation. Drug users often exhibit a strong association with environmental cues associated with drug use, which significantly contribute to relapse triggers.[12] The CPP paradigm serves as a widely utilized animal model for elucidating the underlying mechanisms of associative learning, particularly in the context of drug addiction research.[13] In our investigation, subanesthetic doses of ketamine were administered to effectively establish a CPP model in ketamine-addicted rats.

Our findings revealed a decrease in the ALFF values in the hippocampus of ketamine-addicted rats. The concept of ALFF, initially introduced by Professor Zang in 2007,[14] serves as an indicator of spontaneous neural activity in local brain areas. Additionally, H&E staining showed evidence of apoptosis or a tendency toward apoptosis in the hippocampal neurons of ketamine-addicted rats, indicating the significant involvement of the hippocampus in ketamine addiction. Drug addiction is a complex brain disorder characterized by aberrant memory and learning processes. Notably, the hippocampus plays a crucial role in the modulation of memory and cognitive function and is closely associated with gut microbiota.[15,16] Studies have demonstrated that prolonged exposure to ketamine for over 6 months can induce neurotoxic effects on the hippocampus through apoptotic pathways.[17] Ketamine has been shown to enhance apoptosis of hippocampal neurons by affecting tumor necrosis factor, interleukin-1β, interleukin-6, and mitogen-activated protein kinase (MAPK) signaling pathways.[18,19]

The gut microbiota significantly contributes to research on drug addiction. Studies have indicated that both opium[20] and heroin[21] can induce changes in the composition and diversity of gut microbiota in mice. Moreover, exposure to morphine, whether short-term or long-term, has been associated with alterations in gut microbial composition and an increase in pathogenic bacterial communities.[22–25] In this study, fecal metagenomic sequencing was employed to analyze changes and biological characteristics of gut microbiota and revealing differential microbiota composition in ketamine-addicted rats. The results indicated that, at the genus level, the predominant microbiota of the ketamine-addicted rats included Proteus, Brachybacterium, and Akkermansia, suggesting that ketamine addiction induces alterations in the composition of gut microbiota in rats, characterized by an increase in pathogenic bacteria and a decrease in probiotics.

The current study has unveiled that ketamine-addicted rats manifest shortened ileal villi and thinner colonic mucosa, indicative of compromised intestinal barrier function. These experimental findings align with prior research demonstrating that alcohol, cocaine, and morphine can disrupt gut microbiota and compromise intestinal barrier integrity.[26–29] Furthermore, we observed a correlation between the abundance of characteristic gut microbiota in ketamine-addicted rats and ileal villus length as well as colonic mucosal thickness. Indeed, maintaining gut microbial homeostasis is critical for preserving the functional integrity of the intestinal barrier.[25,30]

Previous studies have highlighted that the consumption of substances such as opium, alcohol, and cocaine is associated with dysbiosis of gut microbiota, leading to alterations in intestinal permeability.[8] Additionally, Lactobacillus reuteri, a probiotic crucial for intestinal epithelial

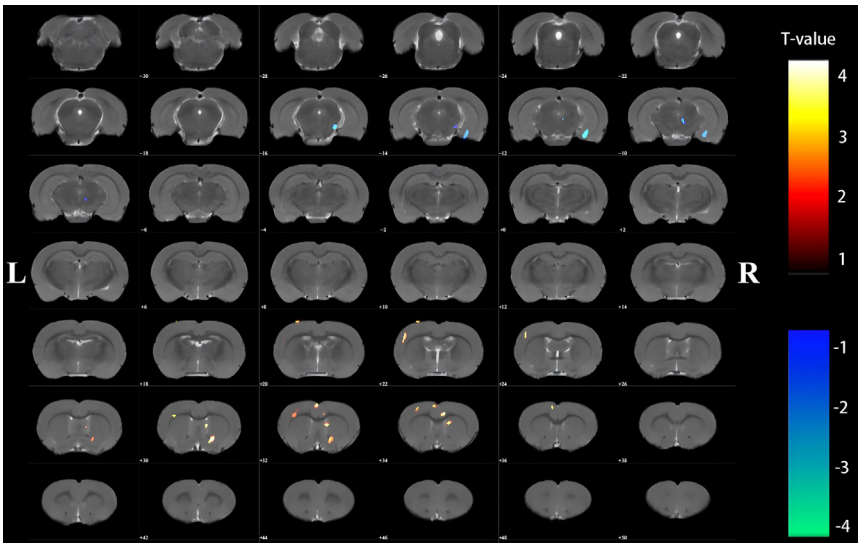

Figure 2. Brain regions with significant difference in ALFF value of resting-state fMRI by two sample t tests between the two groups in rats (n = 7/7)
Hot colors represent higher ALFF values in the ketamine addiction group than in the saline control group, and cool colors represent the lower ALFF values in the ketamine addiction group than in the control group. $p < 0.005$, cluster level>20; L, left; R, right.

regeneration and maintenance of intestinal barrier function, was significantly reduced in morphine-addicted mice.[31] It is plausible that ketamine addiction may induce an imbalance in gut microbiota, characterized by an increase in pathogenic bacteria and a decrease in probiotics, contributing to intestinal barrier dysfunction.

Alterations in gut microbiota composition impact hippocampal-dependent learning and memory processes.[32] Our findings suggest a correlation between gut microbiota abundance and hippocampal ALFF values in ketamine-addicted rats, indicating that gut microbiota dysbiosis may directly or indirectly influence hippocampal function. Moreover, brain-derived neurotrophic factor (BDNF) plays a crucial role in regulating spatial learning, memory, and cognitive function, as well as in neuronal growth, differentiation, and synaptic formation.[33] BDNF activates various signaling pathways including the MAPK pathway, phospholipase, and phosphatidylinositol 3-kinase pathways, thereby modulating neuronal excitability, synaptic connectivity, and gene expression.[34–37] Sudo et al.[38] discovered that germ-free mice exhibited lower levels of BDNF in the hippocampus compared to the normal control group, suggesting that gut microbiota can influence BDNF regulation in the brain. Dysbiosis of gut microbiota disrupts BDNF expression in the hippocampus, leading to functional disturbances and structural changes, ultimately resulting in emotional and cognitive impairments.[39,40]

Lipopolysaccharide (LPS), produced by gram-negative bacteria, is a significant mediator in the influence of the gut microbiota on the brain and host behavior. It is also one of the most abundant and potent activators of innate immune signaling.[41] An imbalance in intestinal flora leads to the secretion of LPS, which regulates inflammatory signaling pathways promoting neuroinflammation and neuronal injury. Previous studies have shown that intestinal mucosal dysfunction increases the translocation of gram-negative bacteria or LPS from the intestine to the circulatory system.[42] LPS binds to the microglial pattern recognition receptor Toll-like receptor 4 (TLR4), inducing microglial activation, which subsequently affects addictive behavior.[43] The pro-inflammatory cytokines produced by the activation of TLR4 and nuclear factor κB (NF-κB) can influence the expression and regulation of neurotransmitters and receptors, leading to the neurodegeneration of dopamine neurons.[44,45] By producing pro-inflammatory factors such as interleukin-1β, interleukin-6, and tumor necrosis factor alpha, activated microglia promote neurodegeneration and impact brain function.[46,47]

Furthermore, the results revealed correlations between the abundance of characteristic gut microbiota in ketamine-addicted rats and ileal villus length, hippocampal ALFF value, and CPP score. Additionally, the length of ileal villi was found to be correlated with hippocampal ALFF value. Previous studies have demonstrated that morphine can elevate levels of pro-inflammatory cytokines such as interleukin-6, interleukin-1β, and tumor necrosis factor alpha.[48] Neuroinflammation plays a critical role in the development of morphine addiction, and modulation of neuroinflammation can effectively attenuate the rewarding effects associated with morphine addiction.[49] Notably, gut microbiota can regulate intestinal permeability and modulate the neuroinflammatory response. Variations in intestinal barrier function, reduction of short-chain fatty acids, elevation of systemic inflammation, and onset of neuroinflammation may directly or indirectly influence brain function, consequently altering associated addictive behaviors.[28,29,50] Therefore, we hypothesize that gut microbiota dysbiosis and concurrent gut barrier dysfunction in rats with ketamine addiction may contribute to the development of ketamine-conditioned place preference by influencing hippocampal function.

In conclusion, this study provides evidence that ketamine induces gut microbiota dysbiosis and barrier dysfunction and abnormal changes in brain functional activity in CPP model rats. The abundance of gut microbiota associated with CPP score, hippocampal ALFF value, length of ileum villi, and thickness of colonic mucosa, and the decreased ALFF value of the hippocampus was negatively correlated with the ileal villus

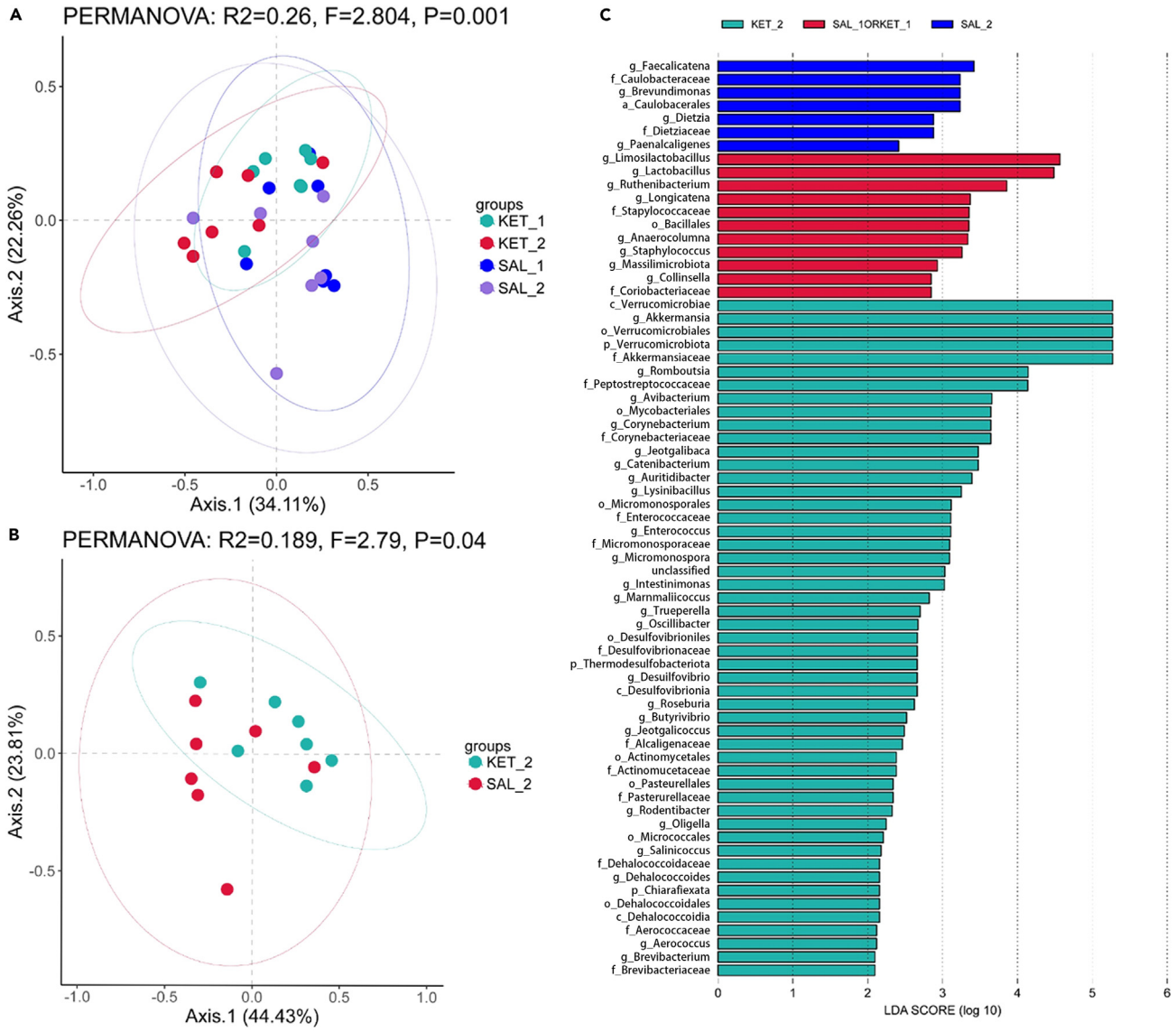

Figure 3. Results of PCoA analysis of the microbial community composition and linear discriminant analysis effect size (LEfSe) analysis of bacteria at genus level in the two groups before and after CPP modeling (n = 7/7)

(A) PCoA analysis results of the microbial community composition in the KET and SAL groups before and after CPP modeling ($p < 0.01$).

(B) PCoA analysis results of the microbial community composition in the KET and SAL groups after CPP modeling ($p < 0.05$).

(C) LEfSe analysis result of bacteria at genus level in the KET and SAL groups before and after CPP modeling ($p < 0.01$). Each transverse column represents a specific species, and the length of the column is proportional to the linear discriminant analysis(LDA) score, with higher values indicating more significant differences. SAL_1, the saline control group before CPP modeling; KET_1, the ketamine addiction group before CPP modeling; SAL_2, the saline control group after CPP modeling; KET_2, the ketamine addiction group after CPP modeling. Abscissa and ordinate represent the first principal component (Axis1) and the second principal component (Axis2), respectively, and the percentage represents the contribution of the component to the difference of the sample.

length. Our findings provide potential avenues for further exploration of the causal correlation between gut microbiota and intestinal barrier and brain and offer preliminary insights into the mechanism of the microbiota-gut-brain axis of ketamine addiction.

Limitations of the study

There are several limitations to this study. First, in this study, we use the CPP model, which can avoid the impact of antibiotic use on the composition of gut microbiota of rats after jugular vein catheterization surgery in the SA model. However, in CPP model, animals passively receive drug reinforcement and cannot simulate human addictive behavior as well as SA model. Therefore, simple CPP experiments cannot

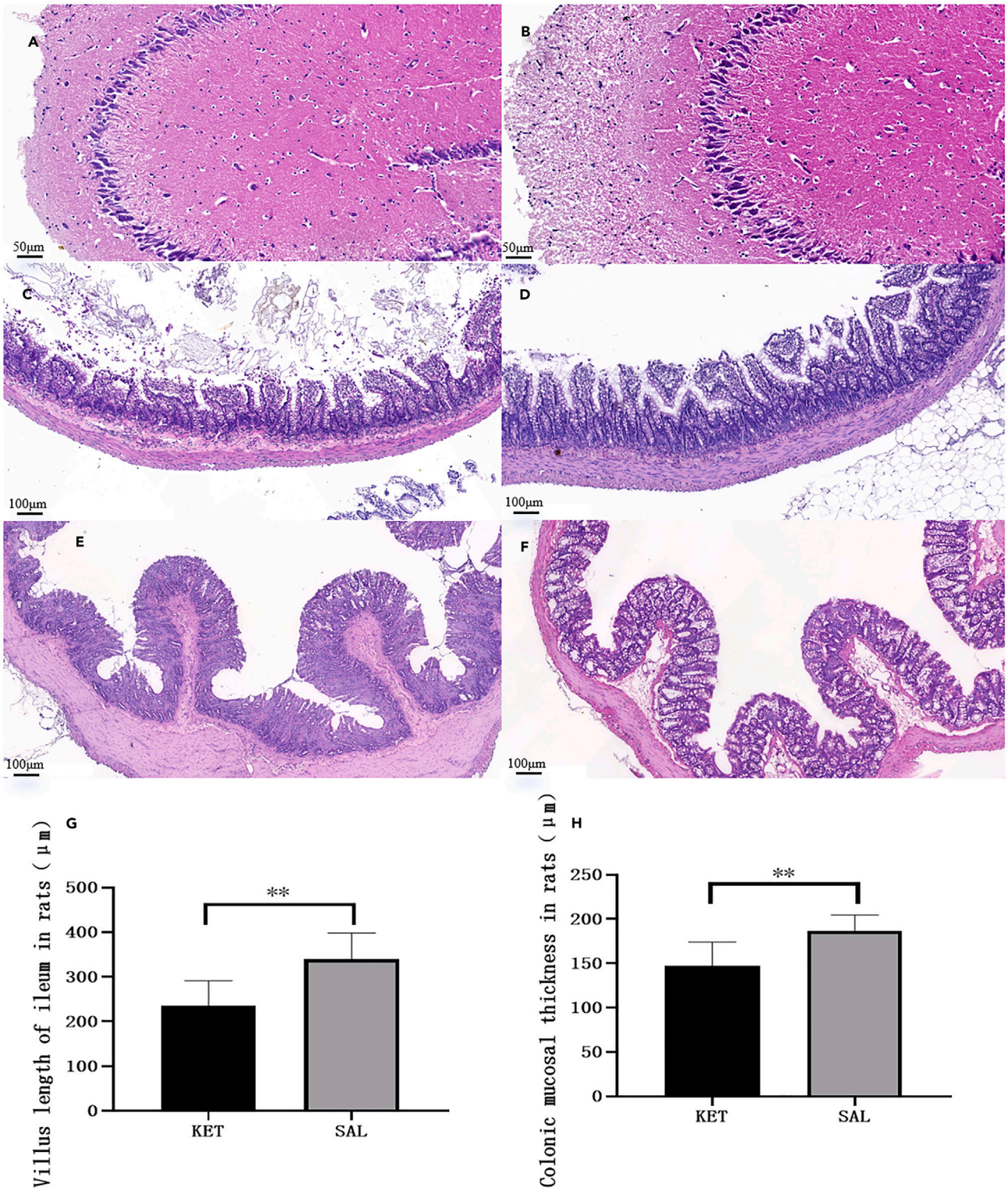

Figure 4. Hematoxylin- and eosin (H&E) staining of the hippocampal neurons and intestinal mucosa in rats between the two groups (*n* = 7/7)

(A) Morphology of hippocampal neurons in KET group (scale bar = 50 μm).

(B) Morphology of hippocampal neurons in SAL group (scale bar = 50 μm).

(C) Morphology of ileal villi in KET group (scale bar = 100 μm).

(D) Morphology of ileal villi in SAL group (scale bar = 100 μm).

Figure 4. *Continued*

(E) Morphology of colonic mucosa in KET group (scale bar = 100 μm).

(F) Morphology of colonic mucosa in SAL group (scale bar = 100 μm).

(G) Compared to the control group, rats in the ketamine group exhibited a statistically significant decrease in the length of ileum villus and a thinner colon mucosa ($p < 0.01$).

(H) Compared to the control group, rats in the ketamine group exhibited a thinner colon mucosa ($p < 0.01$). The data were analyzed by two sample t tests and shown as the mean ± SD, $^{**}p < 0.01$. KET, ketamine; SAL, saline.

explain drug seeking and medication behavior well. In future research, we will further optimize the experimental program, fully utilizing the advantages of self-administering addictive rat models while avoiding the impact of surgical use of antibiotics on the study. Second, this study is only a simple correlation analysis, and due to the lack of mechanism validation experiments like fecal microbiota transplantation (FMT) or antibiotic treatment, which cannot imply causal relationships and specific mechanisms, we will further expand the sample size and consider incorporating Mendelian randomization analysis in our future research, and we should incorporate mechanistic and longitudinal treatment experiments, such as, use an FMT or antibiotic treatment approach to manipulate the gut microbiota in the rats or to investigate whether vagotomy can affect the changes of the microbiota-gut-brain axis in ketamine-addicted rats as vagus nerve plays a role in it. However, because females may respond differently compared with males to drug-related cues and drug use, the gut microbiota and the local brain functional activity and c-Fos expression should also be tested in females. Finally, the rats in our study underwent resting-state fMRI scans under anesthesia, which may affect changes in brain-oxygen-dependent BOLD signals. Future optimization of anesthesia protocols could further validate our research findings.

RESOURCE AVAILABILITY

Lead contact

Further information and requests for resources and reagents should be directed to and will be fulfilled by the lead contact, Professor Shuhua Ma (shma@stu.edu.cn).

Materials availability

This study did not generate new unique reagents.

Data and code availability

- Metagenomic sequencing data have been deposited at Mendeley Data and are publicly available as of the date of publication. Accession numbers are listed in the key resources table. These accession numbers for the datasets are also listed in the key resources table.
- This paper does not report original code.
- Any additional information required to reanalyze the data reported in this paper is available from the lead contact upon request.

ACKNOWLEDGMENTS

This work was supported by the grants from the National Natural Science Foundation of China (Grant numbers 82274657, 82004468); Natural Science Foundation of Guangdong Province of China (Grant number 2024A1515010813); and China Postdoctoral Science Foundation (Grant number 2019M663021). Thanks to Professor Lin from Shantou University School of Medicine for editing the text of this manuscript. Thanks to Professor Binbin Nie, Institute of High Energy Physics, Chinese Academy of Sciences, for her technical support.

AUTHOR CONTRIBUTIONS

Conceptualization, L.X., Z.L.Z., and B.W.G.; methodology, L.X., Z.L.Z., and B.W.G.; software, L.X. and Z.L.Z.; validation, B.W.G., Y.H.H., Y.B.C., and Y.Y.C.; formal analysis, L.X., Z.L.Z., B.W.G., and Z.K.H.; investigation, Z.L.Z., B.W.G., Y.H.H, X.Y.S., Z.K.H, Z.Q.X., Y.B.C., and Y.Y.C.; resources, R.H.W. and S.H.M.; data curation, Z.L.Z., Y.H.H., and Z.K.H.; writing—original draft, Z.L.Z., B.W.G., and Y.H.H.; writing—review & editing, L.X., Z.L.Z., and X.Y.S.; visualization, L.X. and Z.L.Z.; supervision, R.H.W. and S.H.M.; project administration, L.X. and S.H.M.; funding acquisition, L.X. and S.H.M.

DECLARATION OF INTERESTS

The authors declare no competing interests.

Table 2. Differences in villus length of ileum and colonic mucosal thickness between the ketamine addiction group and saline control group in rats

Index	KET group	SAL group	*P* valve
Villus length of ileum (μm)	235.7 ± 21.0	339.9 ± 22.2	0.005
Colonic mucosal thickness (μm)	147.2 ± 10.2	186.6 ± 6.86	0.007

The data were analyzed by two sample t tests and shown as the mean ± SD. KET, ketamine; SAL, saline.

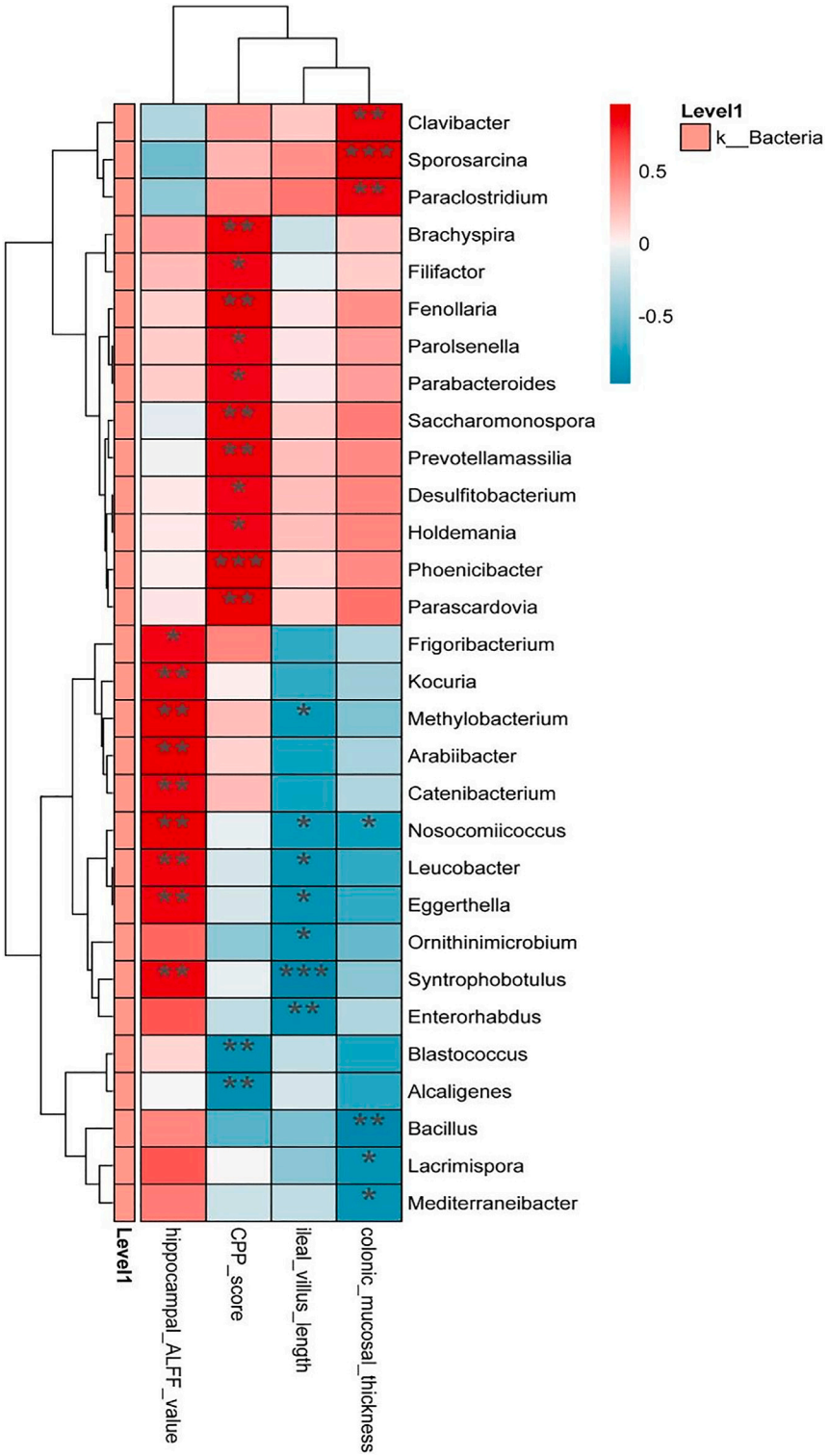

Figure 5. Heatmap of the correlation between horizontal flora abundance at the genus level and CPP score, hippocampal ALFF value, ileal villus length, and colonic mucosal thickness

Spearman or Pearson correlation analysis: The X axis is the related index, and the Y axis is the genus-level flora. The R value (rank correlation) and the *p* value with correction for false discovery rates are calculated. r values are shown in different colors in the figure, and the right legend is a color range of different r values. *$0.01 \leq p < 0.05$, **$0.001 \leq p < 0.01$, ***$p < 0.001$, $n = 7$.

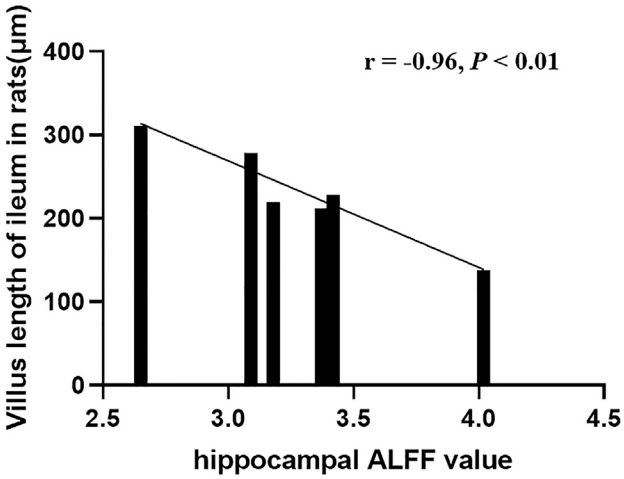

Figure 6. Results of correlation analysis between hippocampal ALFF value and ileal villus length in ketamine addiction rats
(Pearson correlation analysis, $r = -0.96$, $p < 0.01$, $n = 7$).

STAR★METHODS

Detailed methods are provided in the online version of this paper and include the following:

- KEY RESOURCES TABLE
- EXPERIMENTAL MODEL AND STUDY PARTICIPANT DETAILS
  - Animals and groups
  - Conditioned place preference addiction rat model
- METHOD DETAILS
  - MRI image acquisition, data preprocessing and analysis
  - Metagenomic sequencing of rat feces
  - Sampling and HE staining of hippocampal and intestinal tissues
- QUANTIFICATION AND STATISTICAL ANALYSIS

Received: May 12, 2024
Revised: August 2, 2024
Accepted: September 27, 2024
Published: September 30, 2024

REFERENCES

1. Copeland, J., and Dillon, P. (2005). The health and psycho-social consequences of ketamine use. Intern. J. Drug Policy *16*, 122–131. https://doi.org/10.1016/j.drugpo.2004.12.003.
2. Bokor, G., and Anderson, P.D. (2014). Ketamine: an update on its abuse. J. Pharm. Pract. *27*, 582–586. https://doi.org/10.1177/0897190014525754.
3. Chakraborty, K., Neogi, R., and Basu, D. (2011). Club drugs: review of the 'rave' with a note of concern for the Indian scenario. Indian J. Med. Res. *133*, 594–604.
4. Degenhardt, L., Baxter, A.J., Lee, Y.Y., Hall, W., Sara, G.E., Johns, N., Flaxman, A., Whiteford, H.A., and Vos, T. (2014). The global epidemiology and burden of psychostimulant dependence: findings from the Global Burden of Disease Study 2010. Drug Alcohol Depend. *137*, 36–47. https://doi.org/10.1016/j.drugalcdep.2013.12.025.
5. Ogawa, S., Lee, T.M., Kay, A.R., and Tank, D.W. (1990). Brain magnetic resonance imaging with contrast dependent on blood oxygenation. Proc. Natl. Acad. Sci. USA *87*, 9868–9872. https://doi.org/10.1073/pnas.87.24.9868.
6. Febo, M., Segarra, A.C., Nair, G., Schmidt, K., Duong, T.Q., and Ferris, C.F. (2005). The neural consequences of repeated cocaine exposure revealed by functional MRI in awake rats. Neuropsychopharmacology *30*, 936–943. https://doi.org/10.1038/sj.npp.1300653.
7. Capuco, A., Urits, I., Hasoon, J., Chun, R., Gerald, B., Wang, J.K., Kassem, H., Ngo, A.L., Abd-Elsayed, A., Simopoulos, T., et al. (2020). Current Perspectives on Gut Microbiome Dysbiosis and Depression. Adv. Ther. *37*, 1328–1346. https://doi.org/10.1007/s12325-020-01272-7.
8. Salavrakos, M., Leclercq, S., De Timary, P., and Dom, G. (2021). Microbiome and substances of abuse. Prog. Neuro-Psychopharmacol. Biol. Psychiatry *105*, 110113. https://doi.org/10.1016/j.pnpbp.2020.110113.
9. Ren, M., and Lotfipour, S. (2020). The role of the gut microbiome in opioid use. Behav. Pharmacol. *31*, 113–121. https://doi.org/10.1097/FBP.0000000000000538.
10. Meckel, K.R., and Kiraly, D.D. (2019). A potential role for the gut microbiome in substance use disorders. Psychopharmacology (Berl) *236*, 1513–1530. https://doi.org/10.1007/s00213-019-05232-0.
11. Liu, Y., Lin, D., Wu, B., and Zhou, W. (2016). Ketamine abuse potential and use disorder. Brain Res. Bull. *126*, 68–73. https://doi.org/10.1016/j.brainresbull.2016.05.016.
12. Caprioli, D., Celentano, M., Paolone, G., and Badiani, A. (2007). Modeling the role of environment in addiction. Prog. Neuro-Psychopharmacol. Biol. Psychiatry *31*, 1639–1653. https://doi.org/10.1016/j.pnpbp.2007.08.029.
13. Moron, J.A., Gullapalli, S., Taylor, C., Gupta, A., Gomes, I., and Devi, L.A. (2010). Modulation of opiate-related signaling molecules in morphine-dependent conditioned behavior: conditioned place preference to morphine induces CREB phosphorylation. Neuropsychopharmacology *35*, 955–966. https://doi.org/10.1038/npp.2009.199.
14. Zang, Y.F., He, Y., Zhu, C.Z., Cao, Q.J., Sui, M.Q., Liang, M., Tian, L.X., Jiang, T.Z., and

Wang, Y.F. (2007). Altered baseline brain activity in children with ADHD revealed by resting-state functional MRI. Brain Dev. *29*, 83–91. https://doi.org/10.1016/j.braindev.2006.07.002.

15. Olson, C.A., Vuong, H.E., Yano, J.M., Liang, Q.Y., Nusbaum, D.J., and Hsiao, E.Y. (2018). The Gut Microbiota Mediates the Anti-Seizure Effects of the Ketogenic Diet. Cell *174*, 497. https://doi.org/10.1016/j.cell.2018.06.051.
16. Luczynski, P., Moquin, L., and Gratton, A. (2015). Chronic stress alters the dendritic morphology of callosal neurons and the acute glutamate stress response in the rat medial prefrontal cortex. Stress *18*, 654–667. https://doi.org/10.3109/10253890.2015.1073256.
17. Li, Q., Qin, X.Q., Sun, L., Liu, D.X., Zhang, Q., Pan, F., and Yew, D. (2020). Chronic sub-anesthetic ketamine induces permanent hypolocomotion and impairment of hippocampus in adolescent cynomolgus monkeys. Neurosci. Lett. *717*, 134702. https://doi.org/10.1016/j.neulet.2019.134702.
18. Li, M., and Xue, Y. (2021). The upregulation of Nur77 decreases ketamine-induced hippocampal neurons toxicity in rats. Neuroreport *32*, 1370–1378. https://doi.org/10.1097/WNR.0000000000001738.
19. Wu, G.H., Guo, Q.H., Xu, X.D., Lin, J.C., You, G.T., Lin, C.H., and Zhang, L.C. (2023). Ketamine exerts dual effects on the apoptosis of primary cultured hippocampal neurons from fetal rats *in vitro*. Metab. Brain Dis. *38*, 2417–2426. https://doi.org/10.1007/s11011-023-01236-0.
20. Gicquelais, R.E., Bohnert, A.S.B., Thomas, L., and Foxman, B. (2020). Opioid agonist and antagonist use and the gut microbiota: associations among people in addiction treatment. Sci. Rep. *10*, 19471. https://doi.org/10.1038/s41598-020-76570-9.
21. Yang, J., Xiong, P., Bai, L., Zhang, Z., Zhou, Y., Chen, C., Xie, Z., Xu, Y., Chen, M., Wang, H., et al. (2021). The Association of Altered Gut Microbiota and Intestinal Mucosal Barrier Integrity in Mice With Heroin Dependence. Front. Nutr. *8*, 765414. https://doi.org/10.3389/fnut.2021.765414.
22. O'Sullivan, S.J., Malahias, E., Park, J., Srivastava, A., Reyes, B.A.S., Gorky, J., Vadigepalli, R., Van Bockstaele, E.J., and Schwaber, J.S. (2019). Single-Cell Glia and Neuron Gene Expression in the Central Amygdala in Opioid Withdrawal Suggests Inflammation With Correlated Gut Dysbiosis. Front. Neurosci. *13*, 665. https://doi.org/10.3389/fnins.2019.00665.
23. Akbarali, H.I., and Dewey, W.L. (2017). The gut-brain interaction in opioid tolerance. Curr. Opin. Pharmacol. *37*, 126–130. https://doi.org/10.1016/j.coph.2017.10.012.
24. Wang, F., Meng, J., Zhang, L., Johnson, T., Chen, C., and Roy, S. (2018). Morphine induces changes in the gut microbiome and metabolome in a morphine dependence model. Sci. Rep. *8*, 3596. https://doi.org/10.1038/s41598-018-21915-8.
25. Banerjee, S., Sindberg, G., Wang, F., Meng, J., Sharma, U., Zhang, L., Dauer, P., Chen, C., Dalluge, J., Johnson, T., and Roy, S. (2016). Opioid-induced gut microbial disruption and bile dysregulation leads to gut barrier compromise and sustained systemic inflammation. Mucosal Immunol. *9*, 1418–1428. https://doi.org/10.1038/mi.2016.9.
26. Leclercq, S., Matamoros, S., Cani, P.D., Neyrinck, A.M., Jamar, F., Stärkel, P., Windey, K., Tremaroli, V., Bäckhed, F., Verbeke, K., et al. (2014). Intestinal permeability, gut-bacterial dysbiosis, and behavioral markers of alcohol-dependence severity. Proc. Natl. Acad. Sci. USA *111*, E4485–E4493. https://doi.org/10.1073/pnas.1415174111.
27. Chivero, E.T., Ahmad, R., Thangaraj, A., Periyasamy, P., Kumar, B., Kroeger, E., Feng, D., Guo, M.L., Roy, S., Dhawan, P., et al. (2019). Cocaine Induces Inflammatory Gut Milieu by Compromising the Mucosal Barrier Integrity and Altering the Gut Microbiota Colonization. Sci. Rep. *9*, 12187. https://doi.org/10.1038/s41598-019-48428-2.
28. Lee, K., Vuong, H.E., Nusbaum, D.J., Hsiao, E.Y., Evans, C.J., and Taylor, A.M.W. (2018). The gut microbiota mediates reward and sensory responses associated with regimen-selective morphine dependence. Neuropsychopharmacology *43*, 2606–2614. https://doi.org/10.1038/s41386-018-0211-9.
29. Ning, T., Gong, X., Xie, L., and Ma, B. (2017). Gut Microbiota Analysis in Rats with Methamphetamine-Induced Conditioned Place Preference. Front. Microbiol. *8*, 1620. https://doi.org/10.3389/fmicb.2017.01620.
30. Blackwood, B.P., Yuan, C.Y., Wood, D.R., Nicolas, J.D., Grothaus, J.S., and Hunter, C.J. (2017). Probiotic Lactobacillus Species Strengthen Intestinal Barrier Function and Tight Junction Integrity in Experimental Necrotizing Enterocolitis. J. Probiotics Health *5*, 159. https://doi.org/10.4172/2329-8901.1000159.
31. Wu, H., Xie, S., Miao, J., Li, Y., Wang, Z., Wang, M., and Yu, Q. (2020). Lactobacillus reuteri maintains intestinal epithelial regeneration and repairs damaged intestinal mucosa. Gut Microb. *11*, 997–1014. https://doi.org/10.1080/19490976.2020.1734423.
32. Tang, W., Meng, Z., Li, N., Liu, Y., Li, L., Chen, D., and Yang, Y. (2020). Roles of Gut Microbiota in the Regulation of Hippocampal Plasticity, Inflammation, and Hippocampus-Dependent Behaviors. Front. Cell. Infect. Microbiol. *10*, 611014. https://doi.org/10.3389/fcimb.2020.611014.
33. Park, H., and Poo, M.M. (2013). Neurotrophin regulation of neural circuit development and function. Nat. Rev. Neurosci. *14*, 7–23. https://doi.org/10.1038/nrn3379.
34. Vilar, M., and Mira, H. (2016). Regulation of Neurogenesis by Neurotrophins during Adulthood: Expected and Unexpected Roles. Front. Neurosci. *10*, 26. https://doi.org/10.3389/fnins.2016.00026.
35. Huang, E.J., and Reichardt, L.F. (2003). Trk receptors: roles in neuronal signal transduction. Annu. Rev. Biochem. *72*, 609–642. https://doi.org/10.1146/annurev.biochem.72.121801.161629.
36. Chao, M.V. (2003). Neurotrophins and their receptors: a convergence point for many signalling pathways. Nat. Rev. Neurosci. *4*, 299–309. https://doi.org/10.1038/nrn1078.
37. Kaplan, D.R., and Miller, F.D. (2000). Neurotrophin signal transduction in the nervous system. Curr. Opin. Neurobiol. *10*, 381–391. https://doi.org/10.1016/s0959-4388(00)00092-1.
38. Sudo, N., Chida, Y., Aiba, Y., Sonoda, J., Oyama, N., Yu, X.N., Kubo, C., and Koga, Y. (2004). Postnatal microbial colonization programs the hypothalamic-pituitary-adrenal system for stress response in mice. J. Physiol. *558*, 263–275. https://doi.org/10.1113/jphysiol.2004.063388.
39. Bravo, J.A., Forsythe, P., Chew, M.V., Escaravage, E., Savignac, H.M., Dinan, T.G., Bienenstock, J., and Cryan, J.F. (2011). Ingestion of Lactobacillus strain regulates emotional behavior and central GABA receptor expression in a mouse via the vagus nerve. Proc. Natl. Acad. Sci. USA *108*, 16050–16055. https://doi.org/10.1073/pnas.1102999108.
40. Hill, J.M., Bhattacharjee, S., Pogue, A.I., and Lukiw, W.J. (2014). The gastrointestinal tract microbiome and potential link to Alzheimer's disease. Front. Neurol. *5*, 43. https://doi.org/10.3389/fneur.2014.00043.
41. d'Hennezel, E., Abubucker, S., Murphy, L.O., and Cullen, T.W. (2017). Total Lipopolysaccharide from the Human Gut Microbiome Silences Toll-Like Receptor Signaling. mSystems *2*, 10. https://doi.org/10.1128/mSystems.00046-17.
42. Tulkens, J., Vergauwen, G., Van Deun, J., Geeurickx, E., Dhondt, B., Lippens, L., De Scheerder, M.A., Miinalainen, I., Rappu, P., De Geest, B.G., et al. (2020). Increased levels of systemic LPS-positive bacterial extracellular vesicles in patients with intestinal barrier dysfunction. Gut *69*, 191–193. https://doi.org/10.1136/gutjnl-2018-317726.
43. Lewitus, G.M., Konefal, S.C., Greenhalgh, A.D., Pribiag, H., Augereau, K., and Stellwagen, D. (2016). Microglial TNF-alpha Suppresses Cocaine-Induced Plasticity and Behavioral Sensitization. Neuron *90*, 483–491. https://doi.org/10.1016/j.neuron.2016.03.030.
44. Cicchetti, F., Brownell, A.L., Williams, K., Chen, Y.I., Livni, E., and Isacson, O. (2002). Neuroinflammation of the nigrostriatal pathway during progressive 6-OHDA dopamine degeneration in rats monitored by immunohistochemistry and PET imaging. Eur. J. Neurosci. *15*, 991–998. https://doi.org/10.1046/j.1460-9568.2002.01938.x.
45. Qin, L., Wu, X., Block, M.L., Liu, Y., Breese, G.R., Hong, J.S., Knapp, D.J., and Crews, F.T. (2007). Systemic LPS causes chronic neuroinflammation and progressive neurodegeneration. Glia *55*, 453–462. https://doi.org/10.1002/glia.20467.
46. Fan, L.W., Tien, L.T., Zheng, B., Pang, Y., Lin, R.C.S., Simpson, K.L., Ma, T., Rhodes, P.G., and Cai, Z. (2011). Dopaminergic neuronal injury in the adult rat brain following neonatal exposure to lipopolysaccharide and the silent neurotoxicity. Brain Behav. Immun. *25*, 286–297. https://doi.org/10.1016/j.bbi.2010.09.020.
47. Zhou, X., and Spittau, B. (2018). Lipopolysaccharide-Induced Microglia Activation Promotes the Survival of Midbrain Dopaminergic Neurons In Vitro. Neurotox. Res. *33*, 856–867. https://doi.org/10.1007/s12640-017-9842-6.
48. Nakajima, A., Yamada, K., Nagai, T., Uchiyama, T., Miyamoto, Y., Mamiya, T., He, J., Nitta, A., Mizuno, M., Tran, M.H., et al. (2004). Role of tumor necrosis factor-alpha in methamphetamine-induced drug dependence and neurotoxicity. J. Neurosci. *24*, 2212–2225. https://doi.org/10.1523/JNEUROSCI.4847-03.2004.
49. Fujita, Y., Kunitachi, S., Iyo, M., and Hashimoto, K. (2012). The antibiotic minocycline prevents methamphetamine-induced rewarding effects in mice. Pharmacol. Biochem. Behav. *101*, 303–306. https://doi.org/10.1016/j.pbb.2012.01.005.

50. Shen, S., Zhao, J., Dai, Y., Chen, F., Zhang, Z., Yu, J., and Wang, K. (2020). Methamphetamine-induced alterations in intestinal mucosal barrier function occur via the microRNA-181c/TNF-alpha/tight junction axis. Toxicol. Lett. *321*, 73–82. https://doi.org/10.1016/j.toxlet.2019.12.020.
51. Rosen, L.G., Zunder, J., Renard, J., Fu, J., Rushlow, W., and Laviolette, S.R. (2016). Opiate Exposure State Controls a D2-CaMKIIalpha-Dependent Memory Switch in the Amygdala-Prefrontal Cortical Circuit. Neuropsychopharmacology *41*, 847–857. https://doi.org/10.1038/npp.2015.211.
52. Nie, B., Chen, K., Zhao, S., Liu, J., Gu, X., Yao, Q., Hui, J., Zhang, Z., Teng, G., Zhao, C., and Shan, B. (2013). A rat brain MRI template with digital stereotaxic atlas of fine anatomical delineations in paxinos space and its automated application in voxel-wise analysis. Hum. Brain Mapp. *34*, 1306–1318. https://doi.org/10.1002/hbm.21511.
53. Schmieder, R., and Edwards, R. (2011). Quality control and preprocessing of metagenomic datasets. Bioinformatics *27*, 863–864. https://doi.org/10.1093/bioinformatics/btr026.
54. Langmead, B., and Salzberg, S.L. (2012). Fast gapped-read alignment with Bowtie 2. Nat. Methods *9*, 357–359. https://doi.org/10.1038/nmeth.1923.
55. Franzosa, E.A., McIver, L.J., Rahnavard, G., Thompson, L.R., Schirmer, M., Weingart, G., Lipson, K.S., Knight, R., Caporaso, J.G., Segata, N., and Huttenhower, C. (2018). Species-level functional profiling of metagenomes and metatranscriptomes. Nat. Methods *15*, 962–968. https://doi.org/10.1038/s41592-018-0176-y.
56. Kim, J., Kim, M.S., Koh, A.Y., Xie, Y., and Zhan, X. (2016). FMAP: Functional Mapping and Analysis Pipeline for metagenomics and metatranscriptomics studies. BMC Bioinf. *17*, 420. https://doi.org/10.1186/s12859-016-1278-0.
57. Zhu, W., Lomsadze, A., and Borodovsky, M. (2010). Ab initio gene identification in metagenomic sequences. Nucleic Acids Res. *38*, e132. https://doi.org/10.1093/nar/gkq275.
58. Segata, N., Izard, J., Waldron, L., Gevers, D., Miropolsky, L., Garrett, W.S., and Huttenhower, C. (2011). Metagenomic biomarker discovery and explanation. Genome Biol. *12*, R60. https://doi.org/10.1186/gb-2011-12-6-r60.

STAR★METHODS

KEY RESOURCES TABLE

REAGENT or RESOURCE	SOURCE	IDENTIFIER
Biological samples		
Conditioned place preference model of ketamine addiction	Male Sprague-Dawley Rats (6–8 weeks old)	N/A
Chemicals, peptides, and recombinant proteins		
Ketamine Hydrochloride	National Institutes for Food and Drug control	Cat#1867-66-9
Isoflurane	RWD Life Science Co.	Cat#26675-46-7
0.9% saline solution	Kelun	N/A
75% ethanol	Nanchang Likang	N/A
Absolute ethanol	Nanchang Likang	Cat#64-17-5
4% paraformaldehyde fixative solution	Solarbio	Cat#30525-89-4
Hematoxylin	Wexis	Cat#517-28-2
Eosin	Wexis	Cat#17372-87-1
Neutral resin	Lisheng	Q/YSQN41-91
Xylene	Xunye	Cat#1330-20-7
Critical commercial assays		
Cetyltrimethylammonium bromide	Nobleryder	N/A
PCR Master Mix with GC Buffer	New England Biolabs	Cat#M0531S
DNA polymerase	New England Biolabs	Cat#M0530S
DNA Library Prep Kit for Illumina	New England Biolabs	Cat#E7370L
Deposited data		
Metagenomic sequencing data	This paper	http://www.doi.org/10.17632/kpxxc62pyz.1
BOLD-fMRI data	This paper	Shared upon request by the lead contact
Histological staining techniques data	This paper	Shared upon request by the lead contact
Software and algorithms		
MATLAB	MathWorks	https://matlab.p2hp.com/
SPM 12	University College Londo	https://www.fil.ion.ucl.ac.uk/spm/
GRETNA	Beijing Normal University	https://www.nitrc.org/projects/gretna/
ITK-SNAP 3.8	PICSL	https://www.itksnap.org/
Illumina NovaSeq	Illumina	https://www.illumina.com/
Kneaddata	The Huttenhower Lab	https://huttenhower.sph.harvard.edu/kneaddata/
Bowtie2	Johns Hopkins University	http://bowtiebio.sourceforge.net/bowtie2/
Kraken2	CBCB	https://ccb.jhu.edu/software/kraken2/
Image-Pro Plus 6.0	Media Cybernetics	https://analytical-online.com/
Online platform of Wekemo	Wekemo	https://www.bioincloud.tech/
SPSS Statistics 26	IBM	https://www.ibm.com/

EXPERIMENTAL MODEL AND STUDY PARTICIPANT DETAILS

Animals and groups

Healthy Sprague-Dawley (SD) rats (all males, aging 6–8 weeks and weighing 180−250 g) were obtained from the Laboratory Animal Center of Shantou University Medical College. Rats were housed under controlled conditions with a humidity level of 60% ± 5%, room temperature maintained between 20°C and 24°C, a 12-h light-dark cycle, and group housing of 3–5 rats per cage with *ad libitum* access to food and water. The rats were randomly divided into two groups: the katmine addiction group (KET group) and the saline control group (SAL group), each

group consisting of 7 rats. All animal experimental procedures were conducted in compliance with the Regulations of the People's Republic of China for the Administration of Laboratory Animals and followed the guidelines established by the Animal Experiment Ethics Committee of Shantou University Medical College (No.SUMC2022-134).

Conditioned place preference addiction rat model

Ketamine used in this study was procured from the National Institutes for Food and Drug Control, and its use was approved by both the Guangdong Drug Administration and Shantou Market Supervision Administration. A 0.4 mg/mL solution of ketamine hydrochloride was prepared to meet the experimental requirements.

To establish a rat model of ketamine addiction, the conditioned place preference (CPP) paradigm was employed, following the methodologies outlined by Rosen et al.[51] On the first day, rats were allotted 15 min for environmental acclimatization, during which they freely explored the three chambers of the apparatus. On the subsequent day, as part of the baseline preference assessment, rats received a 1 mL/kg saline injection via the tail vein and were allowed to explore for 15 min, while their time spent in each chamber was recorded. Chambers displaying a significant preference were designated as the drug-paired chamber. Rats spending more than 80% of their total time in one chamber were excluded from the study. Thereafter, on days 3, 5, 7, 9, and 11, rats were administered ketamine solution at a dose of 30 mg/kg via the tail vein and placed in the drug-paired chamber for 45 min. On days 4, 6, 8, 10, and 12, rats received an equivalent volume of normal saline and were placed in the non-drug-paired chamber for the same duration. Day 13 involved conducting conditioned preference tests using procedures similar to those of day 2. The CPP score was calculated as the time spent in the drug-paired chamber post-conditioning minus the time spent in the drug-paired chamber during the baseline preference test.

METHOD DETAILS

MRI image acquisition, data preprocessing and analysis

Brain MRI images were collected after CPP models were established. The rats were anesthetised with 1.5–2% isoflurane mixed with oxygen at a flow rate of 0.5–1 L/min and placed into the animal scaffold inside the volume coil of an Agilent 7.0-T MRI scanner. The brain was fixed with a special surface coil designed for rats. Respiration and heart rates were monitored using an MRIcompatible small animal monitoring system (SAII Technologies, Memphis, TN), and the structural and functional images of the rat brain were obtained. The location maps of the three imaging planes were obtained during scanning. (1) The T2-weighted image as the structural phase using fast spin-echo (FSE) sequence with the following parameters: repetition time (TR) = 3000 ms, echo time (TE) = 30 ms, repetitions = 1, field of view (FOV) = 38 × 38 mm^2, matrix size = 128 × 128, slice thickness = 1 mm, interslice gap = 0.1 mm, and 22 continuous slices (voxel size = 0.6 × 0.6 × 1mm^3). (2) Spin echo-echo planar imaging (SE-EPI) sequence was used to obtain the resting-state functional MRI images with the following parameters: TR = 3000 ms, TE = 25.16 ms, repetitions = 240, FOV = 38 × 38 mm^2, matrix size = 64 × 64, slice number = 24, slice thickness = 1 mm, slice gap = 0.1 mm, and 22 continuous slices (voxel size = 0.3 × 0.3 × 1 mm^3).

Data preprocessing was performed with the Statistical Parametric Mapping 12 (SPM12) toolbox on the Matrix Laboratory(MATLAB) 2014b platform. The Digital Imaging and Communications in Medicine (DICOM) images were converted into Neuroimaging Informatics Technology Initiative (NIfTI) format with dcm2nii toolkit and excluded the first 20 time points from further processing. The voxel size of the NIfTI images were enlarged by 5 times using SPM12 software. Mean images from each rat were selected as reference files, and the mean maps of all images were computed to generate adaptive templates using the spmAnimalIHEP[52] toolbox in SPM12. This adaptive template was subsequently imported into ITK-SNAP 3.8 software to excise the skull portion and formulate a new adaptive brain template. We overlaid the brain adaptive template onto the average image of rats, followed by alignment with the standard rat template (resampled to a 1.0 × 1.5 × 1.0 mm^3 resolution). Finally, the images were smoothed for further analysis by a full width at half maximum (FWHM) of a Gaussian kernel of 2 mm^3, then linear detrended and filtered within the frequency range of 0.01 Hz–0.08 Hz were conducted.

The amplitude of low-frequency fluctuation (ALFF) values were calculated with REST V1.8 based on MATLAB 2014b. Fast Fourier transform was used to transform the time series of blood oxygen level signal of each voxel to the frequency domain. The power spectrum of each voxel was acquired from the frequency band, and the averaged square root of the power spectrum in different frequency bands was defined as ALFF value.

Metagenomic sequencing of rat feces

On the 2nd and 13th days of the CPP experiment (before and after model establishment), fresh fecal samples were collected from SD rats and stored at −80°C. Subsequent metagenomic analysis was conducted by the Wekemo Tech Group Co., Ltd. Shenzhen China.

The Cetyltrimethylammonium Bromide (CTAB) method was employed to extract genomic DNA from 28 samples, followed by assessment of DNA integrity, purity, and concentration, construction of a DNA library, and sequencing of the qualified library. Raw metagenomic data from 28 samples was generated using the Illumina NovaSeq platform. Due to a certain proportion of low-quality sequencing data being mixed in with the raw sequencing data, it is necessary to preprocess the raw sequencing data using Kneaddata software. In this process, the joint sequences, low-quality sequences with default quality score threshold less than 20, and sequences with final length less than 50bp were removed from the original data. Then use Bowtie2 software to align Clean Data to the host genome, filtering out sequences from the host and obtaining valid sequences for subsequent analysis. The rationality and effectiveness of quality control are ultimately tested by FastQC.[53,54] Sample sequence reads were aligned against the NCBI NT nucleic acid database and RefSeq whole-genome database using

Kraken2 and a custom-built microbial nucleic acid database. Relative abundance was predicted using Bracken. The sequences underwent quality control and de-hosting using HUMAnN2 software before comparison against the UniRef90 protein database using DIAMOND to obtain corresponding annotation information and a relative abundance table.[55–58] Subsequently, principal coordinate analysis (PCoA) and linear discriminant analysis effect size (LEfSe) were performed based on the species abundance table and functional abundance table.

Sampling and HE staining of hippocampal and intestinal tissues

After induction of isoflurane anesthesia, rats were euthanized via cervical dislocation. Whole brains were carefully dissected, with particular attention to hippocampal removal, which was subsequently preserved in a paraformaldehyde solution. Upon exposure of the abdominal cavity, small portions of both ileum and colon were excised, rinsed thoroughly with PBS or normal saline, and then stored in a 4% paraformaldehyde solution. After an 8-hour fixation period, hippocampal, ileal, and colonic tissues were rinsed thoroughly with running water. Tissues were dehydrated using alcohol, cleared with xylene, and embedded in wax. The wax blocks were sectioned, deparaffinized with xylene, rehydrated with alcohol, stained with hematoxylin and eosin, and finally air-dried and sealed.

The morphology of hippocampal neurons, length of jejunum villi, and thickness of the colonic mucous layer were captured using a 3DHISTECH digital section scanning system or a fluorescence microscope with camera function under 20× and 10× magnification, respectively. Intestinal morphological parameters were observed and measured using Image-Pro Plus 6.0 microscopic image analysis software.

QUANTIFICATION AND STATISTICAL ANALYSIS

The Mann-Whitney (U) rank sum test was used to analyze the CPP score using IBM SPSS Statistics 26 statistical software. Two independent sample T-tests were employed to assess the length of ileal villi and the thickness of colonic mucosa. The intergroup ALFF values were evaluated with two independent-sample t test ($P < 0.005$, cluster size > 20). Principal coordinates analysis (PCoA) was used to analyze the composition of the intestinal microbial community, and linear discriminant analysis effect size (LEfSe) was applied to identify characteristic microorganisms in each group. Correlation analysis of these indicators was performed using either the online platform of Wekemo company or IBM SPSS Statistics 26, followed by the creation of a correlation heatmap. The data were presented as Mean ± Standard Deviation (SD). $P < 0.05$ was considered statistically significant.